

Combustion Characteristics and Laminar Flame Speed of Premixed Ethanol-Air Mixtures with Laser-Induced Spark Ignition

Xu, C., Zhong, A., Wang, C., Jiang, C., Li, X., Zhou, K. & Huang, Y.

Published PDF deposited in Coventry University's Repository

Original citation:

Xu, C, Zhong, A, Wang, C, Jiang, C, Li, X, Zhou, K & Huang, Y 2018, 'Combustion Characteristics and Laminar Flame Speed of Premixed Ethanol-Air Mixtures with Laser-Induced Spark Ignition' *Biofuels Engineering*, vol. 2, no. 1, pp. 63-72.

<https://dx.doi.org/10.1515/bfuel-2017-0005>

DOI 10.1515/bfuel-2017-0005

ISSN 0887-0624

ESSN 1520-5029

Publisher: American Chemical Society

© 2018. This work is licensed under the Creative Commons Attribution-NonCommercial-NoDerivatives 4.0 License. BY-NC-ND 4.0

Copyright © and Moral Rights are retained by the author(s) and/ or other copyright owners. A copy can be downloaded for personal non-commercial research or study, without prior permission or charge. This item cannot be reproduced or quoted extensively from without first obtaining permission in writing from the copyright holder(s). The content must not be changed in any way or sold commercially in any format or medium without the formal permission of the copyright holders.



Research Article

Cangsu Xu, Anhao Zhong, Chongming Wang*, Chaozhao Jiang, Xiaolu Li, Kangquan Zhou, and Yuqi Huang

Combustion Characteristics and Laminar Flame Speed of Premixed Ethanol-Air Mixtures with Laser-Induced Spark Ignition

<https://doi.org/10.1515/bfuel-2017-0005>

Received Nov 30, 2017; accepted Dec 27, 2017

Abstract: Laser-induced spark-ignition (LISI) has an advanced ignition technique with a few benefits over spark ignition. In this study, flame morphology, laminar flame characteristics and combustion characteristics of premixed anhydrous ethanol and air mixtures were investigated using LISI generated by a Q-switched Nd: YAG laser (wavelength: 1064 nm). Experiments were conducted in a constant volume combustion chamber (CVCC) at the initial condition of $T_0=358$ K and $P_0=0.1$ MPa, respectively, and with equivalence ratios (ϕ) of 0.6-1.6. Flame images were recorded by using the high-speed Schlieren photography technique, and the in-vessel pressure was recorded using a piezoelectric pressure transducer. Tests were also carried out with spark ignition, and the results were used as a reference. It has been found that the laminar flame speed of ethanol-air mixtures with LISI was comparable with those of spark ignition, proving that ignition methods have no influence on laminar flame speed which is an inherent characteristic of a fuel-air mixture. The peak laminar burning velocities for LISI and spark ignition with nonlinear extrapolation methods were approximately 50 cm/s at $\phi=1.1$. However, LISI was able to ignite leaner mixtures than spark ignition. The maximum pressure rise rate of LISI was consistently higher than that of spark ignition at all tested ϕ , although the maximum pressure was similar for LISI and spark ignition. The initial combustion duration and main combustion duration reached the minimum at $\phi=1.1$.

Keywords: Laser-induced spark-ignition; Laminar flame speed; Pressure rise rate; Ethanol

*Corresponding Author: **Chongming Wang:** School of Mechanical, Aerospace and Automotive Engineering, Coventry University, Coventry, CV1 5FB, United Kingdom; Email: ac8174@coventry.ac.uk
Cangsu Xu, Anhao Zhong, Kangquan Zhou, Yuqi Huang: College of Energy Engineering, Zhejiang University, Hangzhou, China

1 Introduction

With the increasing consumption of fossil fuels by traditional transportation, the world is facing environment and health problems due to emissions from vehicles. Various technologies have been proposed and studied to solve these problems. Laser ignition has advantages over conventional spark ignition. First of all, the rate of energy deposition, the amount of energy, and the ignition timing can be controlled accurately by using laser ignition [1]. It also allows the flexible location of ignition in the chamber: unlike the spark plug whose intrusion into the cylinder is physically constrained by the geometry of the combustion system, the flexibility of using various optical lenses allows any location of ignition. Moreover, it is possible for laser ignition to achieve multipoint ignition [2, 3].

According to the review of Morsy [1], laser interacts with a combustible mixture via thermal initiation, photochemical ignition, resonant breakdown, and non-resonant breakdown. Currently, the non-resonant breakdown is the most frequently adopted ignition mode to initiate combustion. In recent years, many experiments have been carried out in constant volume combustion chambers (CVCC) to investigate the effect of laser ignition on combustion. Bradley *et al.* [4] employed a Q-switched Nd: YAG laser to study different aspects of laser ignition, including the electrical breakdown, shock-wave generation and propagation, generation of the third lobe, and turbulent flame initiation. Srivastava *et al.* [5] conducted laser ignition of lean hydrogen-air mixtures at an initial temperature of 323 K and an initial pressure of 3 MPa in CVCC, and the results showed that laser ignition caused a higher in-chamber pressure rise rate than spark ignition. It should

Chaozhao Jiang: Loughborough University, Aeronautical and Automotive Engineering, Leicestershire, United Kingdom, LE11 3TU
Xiaolu Li: College of Mechanical and Electrical Engineering, China Jiliang University, Hangzhou, China

be noted that higher pressure rise rate is an indication of faster burning rate, which in most cases is beneficial in improving engine thermal efficiency. However, this could lead to excessive combustion noise and even engine knocking. Kopecek *et al.* [6] studied the main characteristics of methanol-air mixtures with laser ignition under high-pressure high-temperature conditions, and they concluded that leaner mixtures could be ignited successfully by a Q-switched Nd: YAG laser at 1064 nm, as compared to conventional spark ignition. Jiang *et al.* [7] investigate laser ignition in an optical direct injection research engine. They found that the mixture strength significantly affected flame kernel development. Laser-ignition led to reduced ignition delay, faster flame propagation speed and a lower cycle-to-cycle variability than spark ignition. They also found that laser-ignition led to more benefits in the lean conditions compared to stoichiometric or rich conditions.

To reduce engine pollution, promising alternative fuels such as methanol [8], ethanol [9–11] and ethyl acetate [12], have been investigated. Ethanol is an attractive renewable alternative fuel because of its high octane number, and because it has a higher flame propagation velocity than gasoline [13]. However, there are limited data or publications available for the laminar flame speed and combustion characteristics of ethanol-air mixtures which directly compare laser and spark ignition. Thus, in this study, laminar flame characteristics and combustion characteristics of premixed ethanol-air mixtures were investigated using LISI generated by a Q-switched Nd: YAG laser (wavelength: 1064 nm). Experiments were conducted in a constant volume combustion chamber (CVCC) at the initial temperature and pressure of 358 K and 0.1 MPa, respectively, with $\phi=0.6$ –1.6. Flame images were recorded by using the high-speed Schlieren photography technique, and the in-vessel pressure was recorded by using a piezoelectric pressure transducer. Tests were also carried out with spark ignition, and the results were used as a reference. The main novelty of this study is the use of LISI for ethanol-air combustion. Detailed laminar burning characteristics and combustion analysis are provided to reveal the advantages of LISI over spark ignition for ethanol-air combustion.

2 Experimental setup and procedures

2.1 Experimental setup

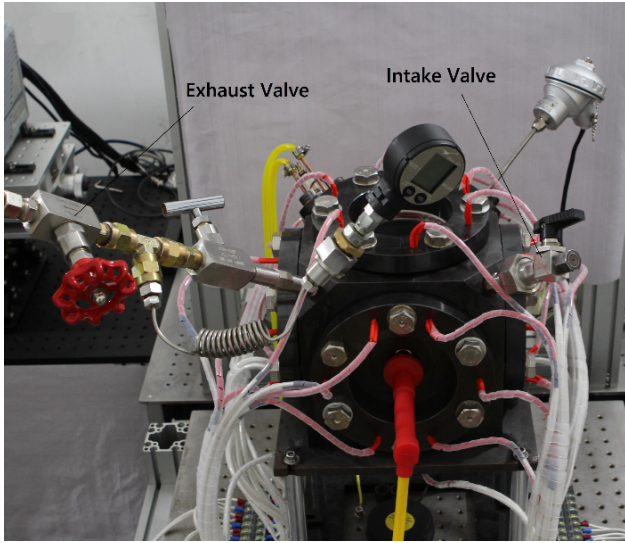
Figure 1 shows the experimental setup used in this investigation. The constant volume combustion chamber (CVCC) has an effective capacity of 1.94 L, and it is capable of withstanding pressure and temperatures up to 20 MPa and 600 K, respectively. Each surface of the CVCC is equipped with six heating elements (the CVCC had 36 heating elements in total) to control the temperature of the CVCC by using a proportional–integral–derivative (PID) controller. For optical access, the CVCC has two pairs of quartz windows with diameters of 105 mm on two opposite sides of the CVCC. A pressure transducer Kistler, Model 6115B) combined with a charge amplifier (Kistler, Type 5018A) was used to measure the dynamic pressure during the combustion process. In the high-speed Schlieren photography system (Figure 1b), flame images were recorded by a high-speed CCD camera (Photron FASTCAM-ultima APX) operating at 6000 fps with a resolution of 512×512 pixels. More details about the experimental apparatus used in this investigation, experiment procedures and experimental uncertainty assessment are provided in previous publications [14–16].

When experiments for the LISI were conducted, the spark ignition system in Figure 1(b) was replaced with the laser ignition system shown in Figure 1(c). A Q-switched Nd: YAG (Dawa-100) laser was used to provide the ignition source, and the laser operated at a wavelength of 1064 nm and with a pulse width of 7.9 ns. The ignition energy can be calculated by the laser energy sensors. In this study, the ignition energy was fixed at 20 mJ at all ϕ . For spark ignition, two opposing platinum electrodes with diameters of 0.4 mm were used as a spark plug along with an ignition coil and a control module.

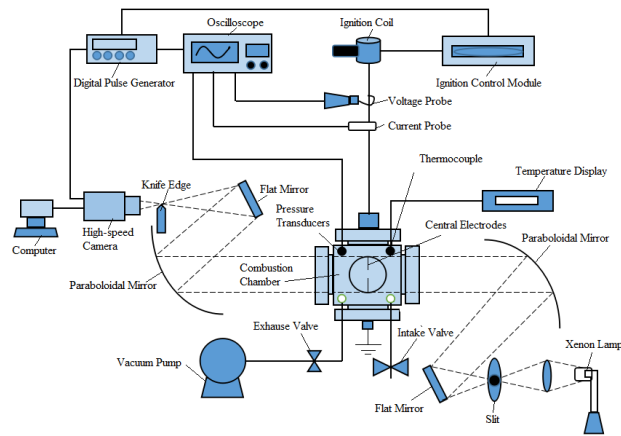
Details about the experimental apparatus used in this investigation can be found in ref [14–16].

2.2 Ethanol and Air

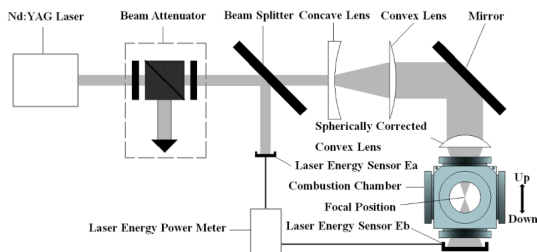
The ethanol used in this study was anhydrous ethanol, the properties of which are listed in Table 1. Filter-cleaned air was dried before it was fed to the combustion chamber. In this study, the $\phi=0.6$ –1.6 is studied to cover the practical flammable air-fuel ϕ and to reflect the typical local ϕ in internal combustion engines.



(a) Constant volume combustion chamber



(b) High-speed Schlieren photography system



(c) Laser-induced ignition system

Figure 1: Experimental setup: (a) constant volume combustion chamber; (b) high-speed Schlieren photography system; (c) laser-induced ignition system

Table 1: Ethanol properties

| Parameters | Ethanol |
|-------------------------------------|---------|
| H/C Ratio | 3 |
| O/C Ratio | 0.5 |
| Gravimetric Oxygen Content (%) | 34.78 |
| Density @ 20°C (kg/m ³) | 790.9 |
| Research Octane Number (RON) | 107 |
| Motor Octane Number (MON) | 89 |
| Stoichiometric Air-Fuel Ratio | 8.95 |
| Lower heating value (LHV) (MJ/kg) | 26.9 |
| LHV (MJ/L) | 21.3 |
| Initial Boiling Point (°C) | 78.4 |

2.3 Data Analysis

According to the background theory behind outwardly propagating spherical flame, the stretched flame speed (S_b) is calculated using:

$$S_b = \frac{dr_f}{dt} \tag{1}$$

where r_f is the flame front radius, and t is the elapsed time after ignition. The stretch rate of the spherical flame (κ), which represents the expanding rate of the flame front area (A), is defined as:

$$\kappa = \frac{d(\ln A)}{dt} = 2 \frac{S_b}{r_f} \tag{2}$$

There are three methods of extrapolating the stretched flame speed to obtain the unstretched flame speed, including one linear method and two nonlinear methods. Generally, the laminar flame speed calculated using nonlinear extrapolation is slightly smaller than that calculated by the linear extrapolation [18, 19]. In many research studies, when compared with the nonlinear methods, the linear method has been used because of its simplicity and because of the low deviations in the results. The linear method can be expressed as:

$$S_b = S_b^0 - L_b \kappa \tag{3}$$

Since the flame propagation process is affected by the stretch, the stretch is thus nonlinear. The nonlinear methods assume adiabatical and quasi-steady flame propagation. The first nonlinear method has been used in Ref. [17]:

$$S_b = S_b^0 - 2S_b^0 L_b / r_f \tag{4}$$

where L_b is the Markstein length.

By combining Equations 2 and 4, the following equation can be used to represent the non-linear relationship

between the stretch rate and the stretched flame propagation speed:

$$S_b = (S_b^0)^2 / S_b^0 + L_b \kappa \quad (5)$$

The second nonlinear method has been used in Ref. [18]:

$$\left(\frac{S_b}{S_b^0}\right)^2 \ln\left(\frac{S_b}{S_b^0}\right) = -2 \frac{L_b \kappa}{S_b^0} \quad (6)$$

Because pressure during the quasi-steady period of combustion can be considered as constant, the laminar burning velocity u_l can be calculated according to the principle of mass conservation [19, 20]:

$$u_l = \frac{\rho_b}{\rho_u} S_b^0 \quad (7)$$

where ρ_b and ρ_u are the adiabatically burned and unburned mixture densities, which can be calculated directly from the EQUIL Code of the Chemkin-Pro software.

The flame thickness is calculated using [18, 19]:

$$\delta_1 = \nu / u_l \quad (8)$$

where ν is the kinetic viscosity of the air-fuel mixture.

The mass fraction burned (MFB) is another important combustion parameter, which has an application of evaluating the combustion process of the engine and guiding the improvement of the combustion system design. MFB is determined from the pressure history data according to the theory described by Rassweiler and Withrow [21]:

$$\text{MFB} = \frac{m_b}{m} = \frac{P - P_0}{P_{\max} - P_0} \quad (9)$$

where m is the total mass of mixture, and m_b is the burned mass of the mixture. The initial combustion duration is defined as the time interval between the spark or laser ignition event and 5% MFB. The main combustion duration is defined as the time interval between 5% and 90% MFB [9].

The calculation of heat release of the combustion of ethanol-air mixtures in the chamber is based on the laws of thermodynamics. the following assumptions are made to simplify the analysis. Firstly, the cylinder charge is considered as an ideal gas; secondly, thermodynamic properties of combustible mixtures inside the chamber are assumed to be uniform; thirdly, dissociation of the combustion products is assumed to be zero. The net heat release rate in the chamber is calculated by using the following equation [22]:

$$\frac{dQ}{dt} = \left(\frac{1}{\gamma - 1}\right) V_c \frac{dP}{dt} + \left(\frac{\gamma}{\gamma - 1}\right) P \frac{dV_c}{dt} \quad (10)$$

where Q is the net heat release, P is the pressure, V_c is the volume of the combustion chamber and t is the time.

In this study, experiments were performed in the constant volume chamber; therefore the net heat release rate can be simplified as:

$$\frac{dQ}{dt} = \left(\frac{1}{\gamma - 1}\right) V_c \frac{dP}{dt} \quad (11)$$

The equation for calculating the net accumulated heat release is:

$$Q = \int_0^t \frac{dQ}{dt} dt \quad (12)$$

where the integral upper limit is the time where the maximum pressure is reached.

2.4 System Uncertainties

The primary errors are due to the uncertainty of initial temperature (ΔU_T), initial pressure (ΔU_P), and flame radius (ΔU_R). The thermocouple has an accuracy of $\pm 0.5\%$, leading to uncertainty of $\sim 0.8\%$ laminar burning velocity at $P_0 = 0.1$ MPa. The accuracy of the pressure sensor is 0.0001 MPa, leading to less than 0.1% laminar burning velocity error. Also, the uncertainty of chamber volume is negligible, leading to a negligible error in air metering. The resolution of syringe used for fuel metering is 5 μL . The uncertainty of flame radius is estimated to be $\sim 1\%$. The global uncertainty of laminar burning velocities is estimated to be within 3%.

3 Results and discussion

In this section, the results and discussion are divided into two subsections: laminar flame characteristics, and combustion characteristics. In each section, the results of LISI are compared with those of conventional spark ignition.

3.1 Laminar burning characteristics

Figure 2 indicates the laminar burning characteristics of both LISI and spark ignition using the three extrapolation methods. The two nonlinear methods led to similar laminar flame characteristics results; however, the linear methods led to an overrated laminar flame speed and Markstein length and an underrated flame thickness. Some discrepancy is observed in Markstein length and flame thickness at the lowest and highest ϕ when using the one linear and two nonlinear methods. This is possibly due to the

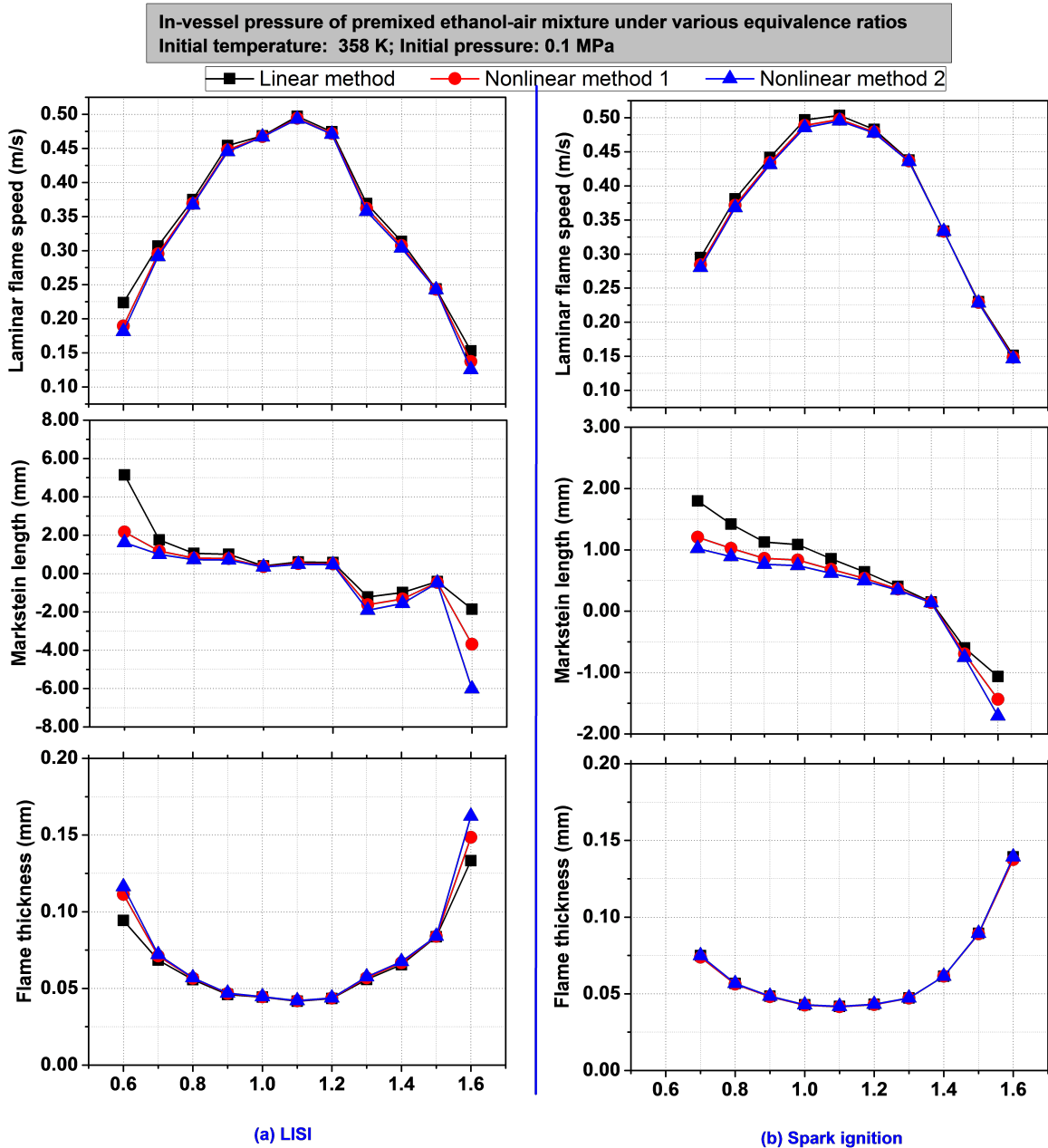


Figure 2: Laminar burning characteristics of premixed ethanol-air mixtures at various equivalence ratios

non-linear relationship between flame propagating speed and stretch rate, especially at extreme lean or rich conditions. This highlights the necessity of using a more accurate non-linear method for data interpretation. The Markstein length is the parameter most affected by the various extrapolation methods. The laminar flame speed of LSI is comparable with spark ignition at the same ϕ . The peak values of laminar burning velocity for the spark ignition and LSI of present work with nonlinear extrapolation were approximately 50 cm/s at $\phi=1.1$. Previous theory [23, 24] indicates that there are two types of flame instabilities: the diffusion-thermal instability and the hydrodynamic instability. The Markstein length results show the influence of stretch rate on the laminar flame speed, which characterises the diffusion-thermal instability [20, 25]. The asymptotic theory [26] shows that the Markstein length is controlled by Lewis number. Markstein length decreases as the mixture becomes rich in heavy hydrocarbon-air

laminar flame speed of LSI is comparable with spark ignition at the same ϕ . The peak values of laminar burning velocity for the spark ignition and LSI of present work with nonlinear extrapolation were approximately 50 cm/s at $\phi=1.1$. Previous theory [23, 24] indicates that there are two types of flame instabilities: the diffusion-thermal instability and the hydrodynamic instability. The Markstein length results show the influence of stretch rate on the laminar flame speed, which characterises the diffusion-thermal instability [20, 25]. The asymptotic theory [26] shows that the Markstein length is controlled by Lewis number. Markstein length decreases as the mixture becomes rich in heavy hydrocarbon-air

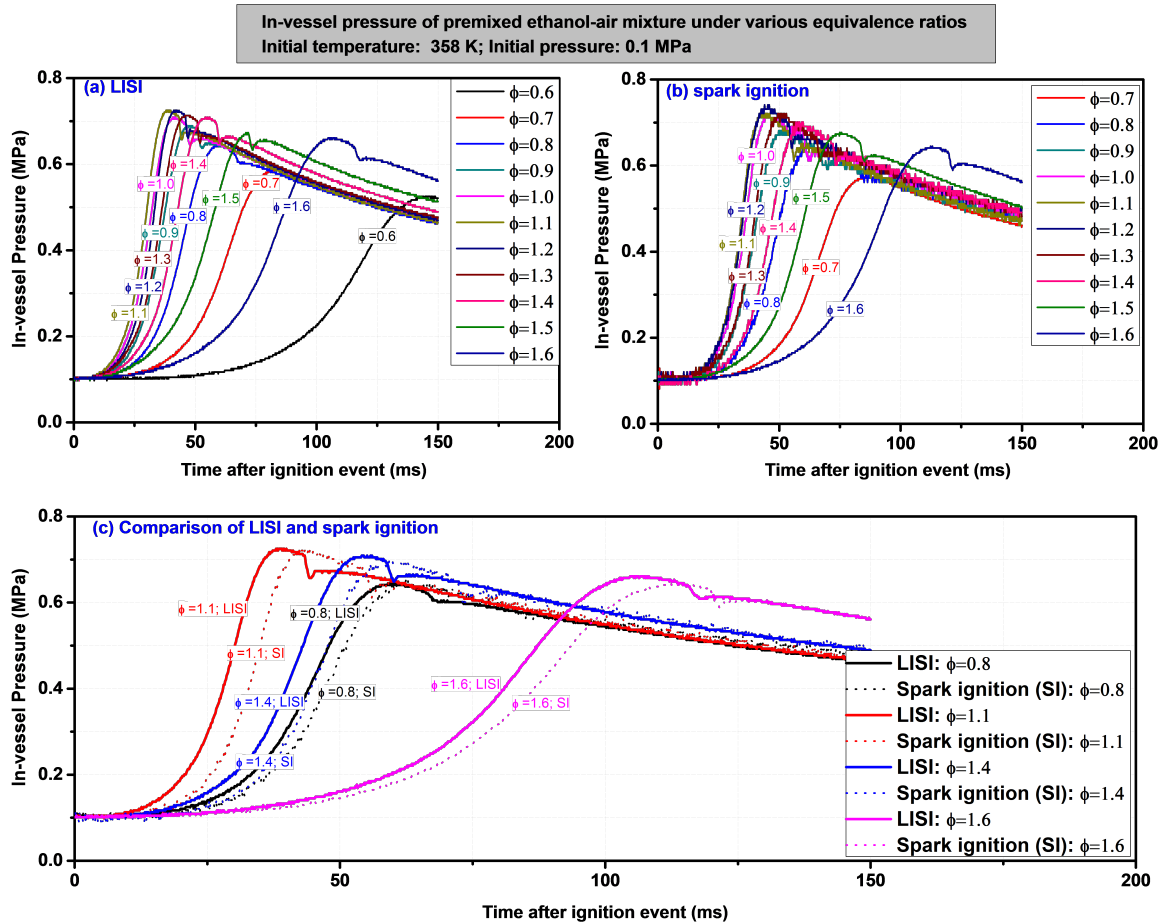


Figure 3: In-vessel pressure of premixed ethanol-air mixtures under various equivalence ratios: (a) LSI; (b) spark ignition; (c) comparison of LSI and spark ignition

mixtures, while the opposite trend is observed for light hydrocarbon-air mixtures [27]. The hydrodynamic instability, which is induced by the density transition across the flame front, is characterised by the flame thickness and the density ratio. A reduced flame thickness reflects this kind of instability. In this study, the Markstein length of heavy hydrocarbon fuel decreased with increases in ϕ , which matched with the theory outlined in Ref. [27]. The flame thickness was smallest at $\phi = 1.1$, indicating that hydrodynamic instability was highest at this ϕ .

It should be noted that for spark ignition, the ethanol-air mixture was not able to be ignited at $\phi = 0.6$.

3.2 Combustion characteristics of LSI

3.2.1 In-vessel Pressure

Pressure history is one of the most important combustion characteristics in internal combustion engines, which can provide relevant information such as peak pressure and pressure rise rate. Figure 3 shows the in-vessel pressure of the premixed ethanol-air mixture under various ϕ . The combustible ϕ range for LSI was 0.6-1.6, which was larger than that of spark ignition (0.7-1.6). For spark ignition experiments, even though ignition energy was increased up to 20 mJ, the premixed ethanol-air mixture failed to be ignited at $\phi = 0.6$. Thus, LSI was able to ignite leaner mixtures than spark ignition. From Figure 3 (a) and Figure 3 (b), it is clear that the pressure history varied significantly with ϕ . $\phi = 1.1$ led to the fastest pressure rise, while too lean or too rich mixtures led to slower pressure rise. Figure 3 (c)

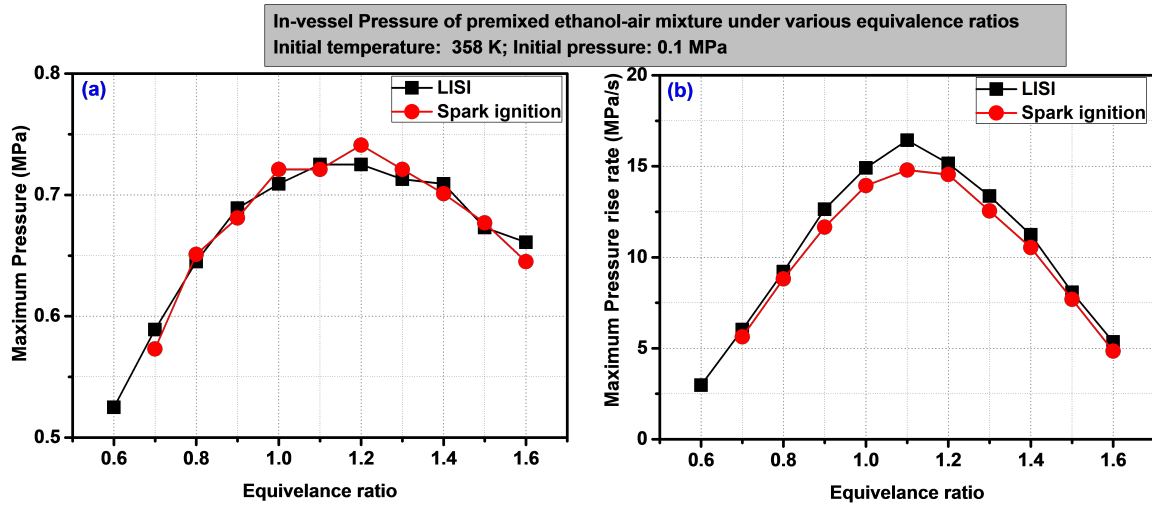


Figure 4: Pressure related parameters during the combustion of premixed ethanol-air mixtures under various equivalence ratios: (a) maximum pressure; (b) maximum pressure rise rate

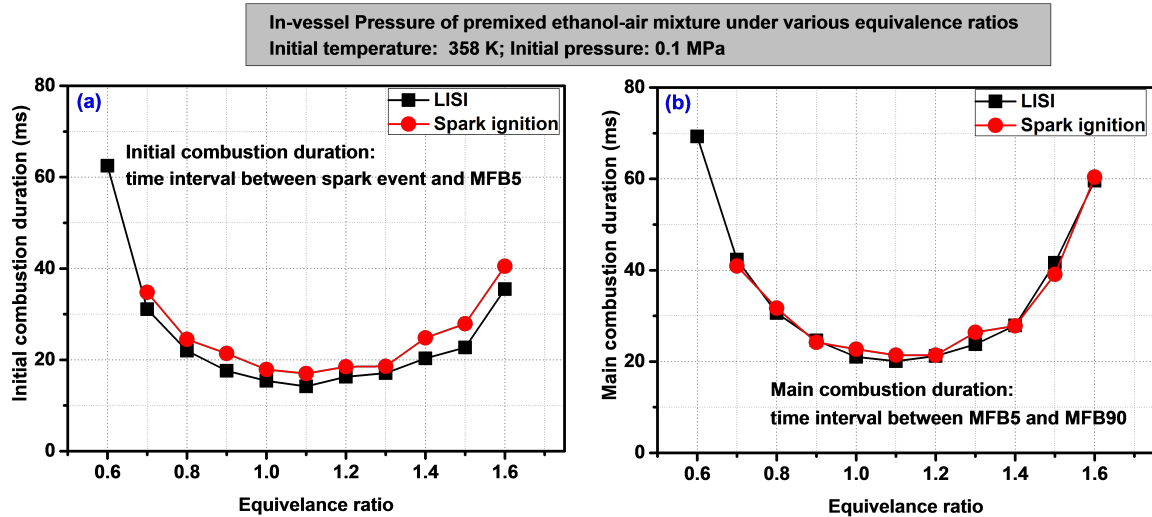


Figure 5: Combustion duration of premixed ethanol-air mixtures under various equivalence ratios: (a) initial combustion duration; (b) main combustion duration

shows that LISI consistently led to an earlier pressure rise than spark ignition, regardless of ϕ .

It can be seen from Figure 3 that there were pressure drops after the peak-pressure. This is due to the heat losses to the combustion chamber wall. Interestingly, after the peak pressure, there was a slight pressure rise in the most of the cases. This can be caused by the tube effect resulting from the installation location and adaptor for the pressure sensor. More detailed experiments are needed to confirm the cause of this phenomenon.

Figure 4 (a) shows the maximum pressure at various ϕ for LISI and spark ignition. For both ignition methods, the maximum pressure increased up to $\phi=1.2$ and then reduced with the further increase of ϕ . In addition, the shape of the maximum pressure was almost symmetrical around $\phi=1.2$. Generally, the maximum pressure of combustion was unaffected by the ignition method. The low peak pressure of the lean mixture was mainly due to the long combustion duration and high heat loss. In addition, the decline of peak pressure for rich mixtures was caused by the

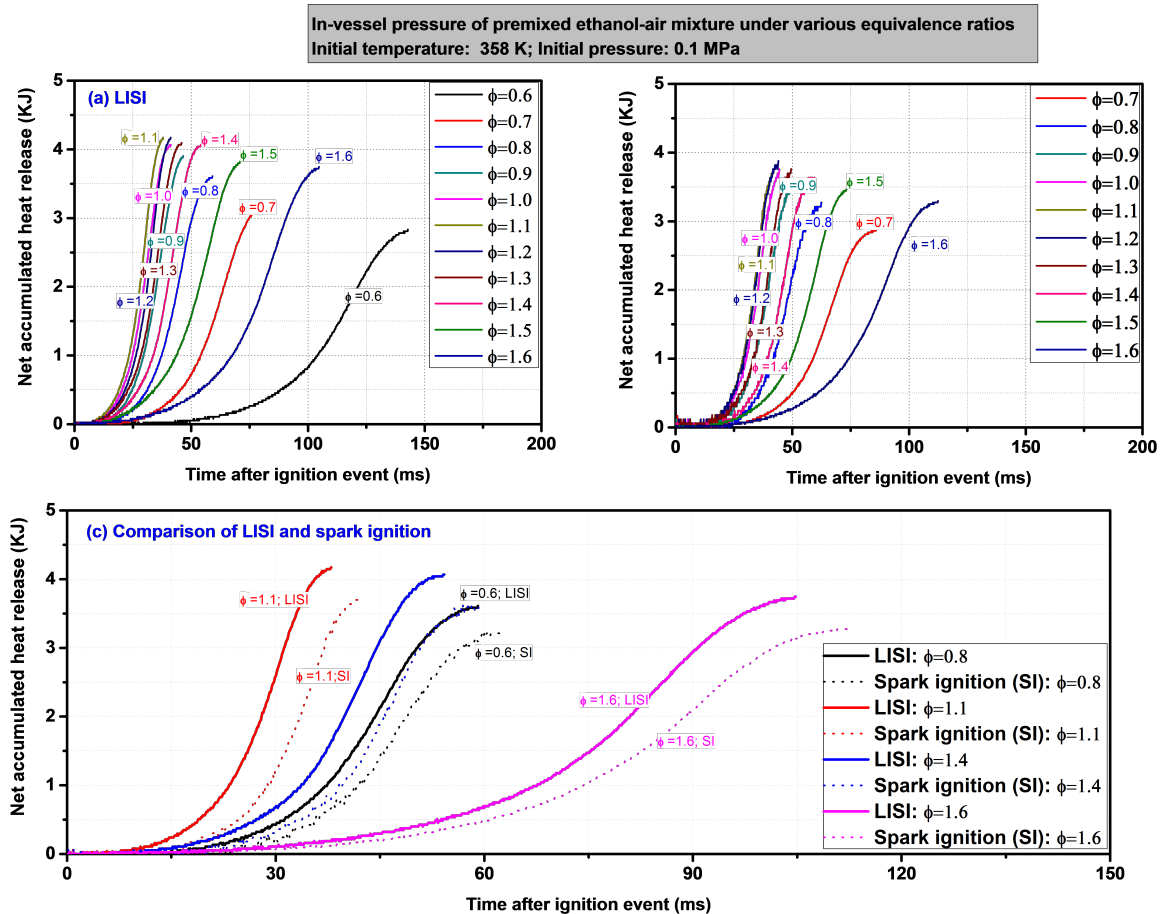


Figure 6: Net accumulated heat release rate of premixed ethanol-air mixture under various equivalence ratios: (a) LISI; (b) spark ignition; (c) comparison of LISI and spark ignition

low amount of oxygen available for combustion, which resulted in incomplete combustion, a long combustion duration and a large mixture specific heat [14].

Pressure rise rate can reflect the burning rate and flame propagation speed of the mixture. Figure 4 (b) shows the pressure rise rate at various ϕ for LISI and spark ignition. For both ignition methods, the pressure rise rate firstly increased up to $\phi=1.1$ and then reduced with the further increase of ϕ . The pressure rise rates for LISI and spark ignition were 16.4 MPa/s and 14.8 MPa/s at $\phi=1.1$, respectively. This is because both rich and lean mixtures lead to lower combustion temperature, and thus, a lower reaction rate [14]. In addition, the shape of the pressure rise rate was almost symmetrical around $\phi=1.1$. Unlike the maximum pressure, the pressure rise rate depended on the ignition methods, with LISI leading to a higher pressure rise rate than spark ignition. For the ethanol-air mixtures with the same ϕ , the pressure rise rate of laser ignition was

slightly higher than that of spark ignition, which means that laser ignition can lead to a higher burning rate, possibly due to the absence of the plasma quenching effect [5].

3.2.2 Ignition delay and combustion duration

Figure 5 shows the initial and main combustion duration versus ϕ . The minimum initial and main combustion durations were obtained at $\phi=1.1$ for LISI, which were 14.2 and 20.1 ms, respectively. Compared to the initial combustion duration under the same ϕ , the main combustion duration was longer, especially for the over lean or rich mixtures. At $\phi=0.6$, the initial combustion duration was significantly longer than that of the other ϕ . For spark ignition, the minimum initial and main combustion durations also appeared at $\phi=1.1$, which were 17.0 and 21.4 ms, respec-

tively. Overall, the initial combustion durations of spark ignition were higher than those of LISI.

3.2.3 Heat release analysis

Figure 6 shows the net accumulated heat release versus time for premixed ethanol-air mixtures with LISI and spark ignition. The slope of the curve represents the rate of heat release. For LISI, $\phi=1.1$ led to the maximum heat release rate. For ϕ ranging from 0.6 to 1.0, the net heat release and rate of heat release increased with increasing ϕ . Under the extremely lean burn condition ($\phi=0.6$), the rate of heat release was apparently lower than those of other conditions. On the other hand, when the $\phi > 1.2$, the net heat release and rate of heat release declined as ϕ was increased, which was due to the incomplete combustion of the mixture. Figure 6(c) shows that LISI consistently led to an earlier heat release, regardless of ϕ .

4 Conclusions

In this study, the combustion characteristics and laminar flame speed of premixed ethanol-air mixtures were investigated using LISI. The experiments were conducted in a CVCC at $T_0=358$ K and $P_0=0.1$ MPa, and $\phi=0.6-1.6$. It was found that the laminar flame speed of ethanol-air mixtures with LISI was comparable with those of spark ignition. This proves that ignition methods have no influence on laminar flame speed which is an inherent characteristic of a fuel-air mixture. LISI was able to ignite leaner mixtures than spark ignition, which implies that LISI is an advanced ignition method for lean combustion, which leads to higher engine thermal efficiency than homogeneous combustion. The maximum pressure of LISI did not show any significant difference as compared to that observed for spark ignition. The pressure rise rate of LISI was consistently higher than that of spark ignition at all tested ϕ , indicating a more robust combustion.

Acknowledgement: This work is supported by the National Basic Research Program (No. 2013CB228106) of China, the National Natural Science Foundation of China (No. 50976100 and 51076138), the Public Beneficial Technology Application Research Project of Science Technology Department of Zhejiang Province (No. 2016C31102 and 2016C31112), the Fundamental Research Funds for the Central Universities of China (No. 2013QNA4017), and the Hangzhou Science Committee (No.20162013A06) of China.

Nomenclature & Abbreviation

| | |
|------------|--|
| δ_l | Flame thickness (mm) |
| γ | Heat capacity ratio |
| ν | Kinetic viscosity (mm^2/s) |
| ϕ | Equivalence ratio |
| A | Flame front area (mm^2) |
| L_b | Markstein length (mm) |
| m_b | Burned mass of mixture (g) |
| m | Total mass of mixture (g) |
| P_{\max} | Peak pressure (MPa) |
| P_0 | Initial pressure (MPa) |
| P | In-vessel pressure (MPa) |
| Q | Net heat release (KJ) |
| r_f | Flame radius (mm) |
| T_0 | Initial temperature (K) |
| u_l | Laminar burning velocity (cm/s) |
| V_c | Volume of chamber (L) |
| CVCC | Constant volume combustion chamber |
| LHV | Lower heating value |
| LISI | Laser-induced spark ignition |
| MON | Motoring Octane Number |
| PID | Proportional–integral–derivative |
| RON | Research Octane Number |

References

- [1] M.H. Morsy, Review and recent developments of laser ignition for internal combustion engines applications, *Renewable and Sustainable Energy Reviews*, 16 (2012) 4849-4875.
- [2] Z. Kuang, E. Lyon, H. Cheng, V. Page, T. Shenton, G. Dearden, Multi-location laser ignition using a spatial light modulator towards improving automotive gasoline engine performance, *Optics and Lasers in Engineering*, 90 (2017) 275-283.
- [3] M. Weinrotter, H. Kopecek, M. Tesch, E. Wintner, M. Lackner, F. Winter, Laser ignition of ultra-lean methane/hydrogen/air mixtures at high temperature and pressure, *Experimental thermal and fluid science*, 29 (2005) 569-577.
- [4] D. Bradley, C. Sheppard, I. Suardjaja, R. Woolley, Fundamentals of high-energy spark ignition with lasers, *Combustion and Flame*, 138 (2004) 55-77.
- [5] D.K. Srivastava, M. Weinrotter, K. Iskra, A.K. Agarwal, E. Wintner, Characterisation of laser ignition in hydrogen–air mixtures in a combustion bomb, *international journal of hydrogen energy*, 34 (2009) 2475-2482.
- [6] H. Kopecek, S. Charareh, M. Lackner, C. Forsich, F. Winter, J. Klausner, et al. Laser ignition of methane-air mixtures at high pressures and diagnostics. ASME 2003 Internal Combustion Engine Division Spring Technical Conference: American Society of Mechanical Engineers; 2003;147-54.
- [7] Y. Jiang, X. Bao, A. Sahu, X. Ma, H. Xu, A. Thong, Flame Kernel Growth and Propagation in an Optical Direct Injection Engine Using Laser Ignition, *SAE Technical Paper 2017-01-2243*, 2017,

- [8] Q. Li, W. Zhang, W. Jin, Y. Xie, Z. Huang, Laminar flame characteristics and kinetic modeling study of methanol-isooctane blends at elevated temperatures, *Fuel*, 184 (2016) 836-845.
- [9] C., Wang, R. Daniel, X. Ma, Comparison of Gasoline (ULG), 2, 5-Dimethylfuran (DMF) and Bio-Ethanol in a DISI Miller Cycle with Late Inlet Valve Closing Time. SAE Technical Paper 2012-01-1147, 2012, <https://doi.org/10.4271/2012-01-1147>.
- [10] C. Wang, S. Zeraati-Rezaei, L. Xiang, H. Xu, Ethanol blends in spark ignition engines: RON, octane-added value, cooling effect, compression ratio, and potential engine efficiency gain, *Applied Energy*, 191 (2017) 603-619.
- [11] C. Wang, A. Janssen, A. Prakash, R. Cracknell, H. Xu, Splash blended ethanol in a spark ignition engine – Effect of RON, octane sensitivity and charge cooling, *Fuel*, 196 (2017) 21-31.
- [12] T. Badawy, J. Williamson, H. Xu, Laminar burning characteristics of ethyl propionate, ethyl butyrate, ethyl acetate, gasoline and ethanol fuels, *Fuel*, 183 (2016) 627-640.
- [13] P. Dirrenberger, P.-A. Glaude, R. Bounaceur, H. Le Gall, A.P. da Cruz, A. Konnov, F. Battin-Leclerc, Laminar burning velocity of gasolines with addition of ethanol, *Fuel*, 115 (2014) 162-169.
- [14] C.-s. Xu, D.-h. Fang, Q.-y. Luo, J. Ma, Y. Xie, X. Zheng, Characterization of gasoline combustion with laser and spark ignition, *Journal of Zhejiang University SCIENCE A*, 16 (2015) 830-838.
- [15] C. Xu, D. Fang, Q. Luo, J. Ma, Y. Xie, A comparative study of laser ignition and spark ignition with gasoline–air mixtures, *Optics & Laser Technology*, 64 (2014) 343-351.
- [16] C. Xu, Y. Hu, X. Li, X. Zhou, A. Zhong, Comparative experimental study of ethanol-air premixed laminar combustion characteristics by laser induced spark and electric spark ignition, *Korean Journal of Chemical Engineering*, (2015) 1-6.
- [17] M. Frankel, G. Sivashinsky, On effects due to thermal expansion and Lewis number in spherical flame propagation, *Combustion science and technology*, 31 (1983) 131-138.
- [18] A.P. Kelley, G. Jomaas, C.K. Law, Critical radius for sustained propagation of spark-ignited spherical flames, *Combustion and Flame*, 156 (2009) 1006-1013.
- [19] X. Ma, C. Jiang, H. Xu, H. Ding, S. Shuai, Laminar burning characteristics of 2-methylfuran and isooctane blend fuels, *Fuel*, 116 (2014) 281-291.
- [20] X.S. Wu, Z.H. Huang, C. Jin, X.G. Wang, B. Zheng, Y.J. Zhang, L.X. Wei, Measurements of Laminar Burning Velocities and Markstein Lengths of 2,5-Dimethylfuran-Air-Diluent Premixed Flames, *Energy & Fuels*, 23 (2009) 4355-4362.
- [21] G.M. Rassweiler, L. Withrow, Motion pictures of engine flames correlated with pressure cards, in, SAE Technical Paper, 1938.
- [22] J.B. Heywood, *Internal combustion engine fundamentals*, McGraw-Hill: New York, 1989.
- [23] C. Law, C. Sung, Structure, aerodynamics, and geometry of premixed flamelets, *Progress in Energy and Combustion Science*, 26 (2000) 459-505.
- [24] M. Matalon, Intrinsic flame instabilities in premixed and non-premixed combustion, *Annu. Rev. Fluid Mech.*, 39 (2007) 163-191.
- [25] X.S. Wu, Q.Q. Li, J. Fu, C.L. Tang, Z.H. Huang, R. Daniel, G.H. Tian, H.M. Xu, Laminar burning characteristics of 2,5-dimethylfuran and iso-octane blend at elevated temperatures and pressures, *Fuel*, 95 (2012) 234-240.
- [26] G.M. Rassweiler, L. Withrow, Motion pictures of engine flames correlated with pressure cards. SAE Technical Paper 380139, 1938, <https://doi.org/10.4271/380139>.
- [27] Bechtold J, M. Matalon, The dependence of the Markstein length on stoichiometry, *Combustion and flame*, 127 (2001) 1906-1913.